

# LIGHT YIELD, IMAGING PROPERTIES AND SPECTRAL RESPONSE OF INORGANIC SCINTILLATORS UNDER INTENSE ION IRRADIATION

E. Gütllich, W. Ensinger, Technical University Darmstadt, Germany

P. Forck, R. Haseitl, B. Walasek-Höhne, GSI Helmholtz Centre for Heavy Ion Research GmbH, Darmstadt, Germany

## Abstract

Scintillating screens are widely used for transverse beam profile monitoring and pepper-pot emittance measurements at accelerator facilities.

For high current beam operations at the GSI heavy ion UNILAC, several inorganic scintillators were investigated under different ion beam conditions. The imaging properties of various materials were studied with respect to light yield and imaged beam width.

The measured properties show a strong dependence on the scintillating material and change significantly with screen temperature. The spectral response of the materials was mapped for different temperature levels, using a spectrometer in the visible and near UV range. The results clearly demonstrate that their temperature behaviour and scintillating properties are critical issues for high current operations and have to be taken into account for correct beam profile reading.

## INTRODUCTION

Scintillating screens are a direct but intercepting method to observe an ion beam. Profile measurements are important for controlling the spatial distribution of the ion beam, as well as the matching of the different parts of the accelerator from the ion source to the experimental area. Depending on beam current and energy, a large variety of scintillating materials can be used.

Additionally scintillating screens are an essential part of a single shot pepper-pot emittance measurement system used for the determination of the width of ‘beamlets’ created by a plate with several small holes. The realization at GSI used for the high current operation of UNILAC is described in [1]. The angular distribution within the phase space can be calculated from the intensity distribution of the ‘beamlets’. The precise measurement of the spot’s light distribution requires a linear light output without saturation effects from the scintillating material and has to match the optical sensitivity of the CCD camera. To observe possible (time dependent) variations of the beam size a short decay time is necessary. The scintillating material has to be radiation hard and it is necessary to ensure that the material is not destroyed by ion beam irradiation during high current operation (see Fig. 1). For precise profile reading the heating of the scintillating material due to the energy loss has to be considered [2].

Several scintillating materials (Table 1) were investigated with different ion beams from protons up to Uranium at energies between 4.8 and 11.4 MeV/u and different beam currents as delivered by the GSI linear

accelerator. Standard scintillators like YAG:Ce or BGO could only be used for low beam currents in the range of some nA [4]. For the high intensity ion beams, ceramic materials and quartz glass have to be applied [2].

Table 1: Investigated materials

Type	Material	Supplier
Crystal scintillator	YAG:Ce, BGO, CdWO <sub>4</sub> , CaF <sub>2</sub> :Eu	Saint Gobain Crystals
Powder	ZnS:Ag	HLW
Ceramics	ZrO <sub>2</sub> :Al, ZrO <sub>2</sub> :Y (YSZ), ZrO <sub>2</sub> :Mg, BN, SiN, SiC, AlN, Al <sub>2</sub> O <sub>3</sub> , Al <sub>2</sub> O <sub>3</sub> : Cr	BCE Special Ceramics
Quartz glass	Herasil 102, SiO <sub>2</sub> :Ce (M382)	Heraeus Quarzglas

## EXPERIMENTAL SETUP

For systematic measurements a movable target ladder (see Fig. 1) with six different scintillating materials was used. This experimental setup allowed to test different materials under identical beam conditions without breaking the vacuum (typical  $5 \cdot 10^{-7}$  mbar).

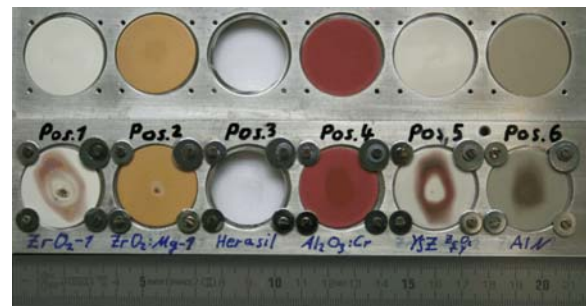


Figure 1: Target ladder with six different scintillating materials before (upper row) and after 100 pulses of U<sup>28+</sup> ion beam (lower row). Beam parameters:  $5.2 \cdot 10^{10}$  particles per pulse (ppp) at 4.8 MeV/u, 0.8 ms pulse length and 0.5 Hz repetition rate. Target modifications after irradiation are visible.

The scintillating screens were monitored with a monochrome CCD camera (AVT Stingray F033B, 8-bit ADC and VGA resolution). Due to the material dependent light yield a lens system with remote controlled iris (Pentax, 25 mm focal length) was implemented. With this experimental setup a resolution of 10 px/mm was achieved. The software BeamView [5] was used for data acquisition. The camera was connected to a PC which runs the server part of BeamView. The images were

recorded and sent to a client application via Ethernet. The reading from an upstream beam current transformer was sent to the client and saved together with the according image for offline analysis.

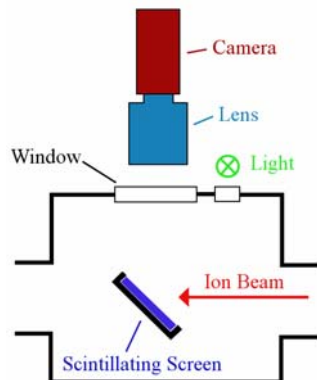


Figure 2: Experimental setup for transverse beam profile monitoring. The target ladder with six scintillating screens is tilted by  $45^\circ$  with respect to the beam and is movable perpendicular to the displayed plane.

The recorded image of the beam spot was projected to both the horizontal and the vertical plane and a quantitative analysis was performed. For the characterisation of the projected beam spots their centre  $\mu$  (1<sup>st</sup> moment) and standard deviation  $\sigma$  (square root of 2<sup>nd</sup> moment which describes beam width) were calculated. The higher statistical moments were also taken into account but are not discussed in this paper [2].

To obtain a reference beam profile with a higher resolution than a Secondary Electron Monitor grid (SEM-grid), a scraper scan (Fig. 3) was implemented in the experimental area.

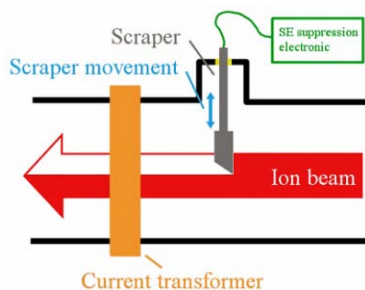


Figure 3: Scheme of the transverse beam profile measurement system based on scraper scan. The scraper is moving through the ion beam and the beam current is measured for each position of the scraper.

Furthermore, spectroscopic studies on the light emitted by the scintillating screens were performed.

The experimental setup (Fig. 4) consists of an imaging spectrograph (Horiba Jobin Yvon CP140-202) coupled to an area scan CCD camera (pco1600). For an object distance of 230 mm, a chromatically corrected UV lens (Linos inspec.x) with a focal length of 50 mm and  $f/2.8$  was chosen. The key issue of this experiment is to have both, the spectral information of the optical transition and

the spatial information about the beam profile along the imaging axis.

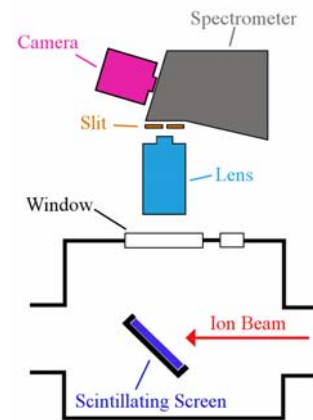


Figure 4: Experimental setup for spectroscopic studies on the light emitted from scintillating materials.

The example in Fig. 5 shows the obtained spectral information for a  $U^{28+}$  ion beam. The AlN sample emits light at 390 nm and the beam profile, along the imaging axis, has a width of approximately 10 mm.

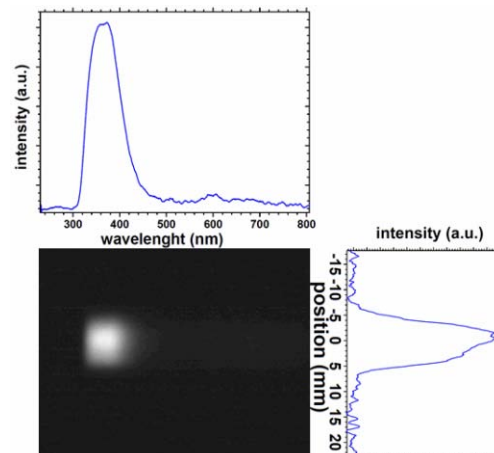


Figure 5: Example of the spectroscopic beam image obtained with  $U^{28+}$  for the AlN sample at 1<sup>st</sup> pulse. Beam parameters:  $5.2 \cdot 10^{10}$  ppp at 4.8 MeV/u and 0.8 ms pulse length.

## RESULTS AND DISCUSSION

### Systematic measurements

For high current operation with an  $Ar^{10+}$  ion beam at 11.4 MeV/u the light yield and beam width were investigated for several materials (Fig. 6).

During irradiation the light yield of AlN,  $ZrO_2:Mg$  and Herasil drops significantly with the integrated particle number. Additionally, the light yield of  $ZrO_2:Mg$  decreases coincidentally with the beam width, but with a different time constant. As reported in [2] the change of the parameters in  $ZrO_2:Al$  is mainly due to the increase of the sample temperature. For  $Al_2O_3$  the light yield and the beam width increase during the irradiation process but

these changes are smaller than for all other investigated materials. The increase of beam width and light yield for  $\text{Al}_2\text{O}_3$  might be due to the heating process.

Most emphasized but difficult to understand are the changes observed for Al doped  $\text{ZrO}_2$  and  $\text{ZrO}_2:\text{Y}$ . As shown in Fig 6. the beam width varies within a factor of two and the major changes of beam width readings are observed for Al and Y doped  $\text{ZrO}_2$  samples. The Herasil sample shows the smallest imaged beam width, whereas AlN shows the maximum width.

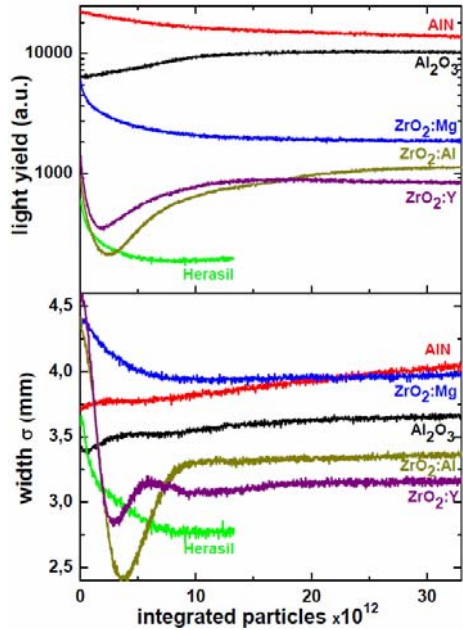


Figure 6: Light yield and beam width over the accumulated ion dose. Each point represents the value for one macro-pulse for different materials irradiated by  $\text{Ar}^{10+}$ . Beam parameters:  $3.3 \cdot 10^{10}$  ppp at 11.4 MeV/u, 0.2 ms pulse length and 1.5 Hz repetition rate.

*Comparison of the methods*

Three different transverse profile measurement methods:  $\text{Al}_2\text{O}_3$  screen, SEM-grid and the scraper scan were compared. The SEM-grid and the scraper were installed 25 cm in front of the scintillating screens holder.

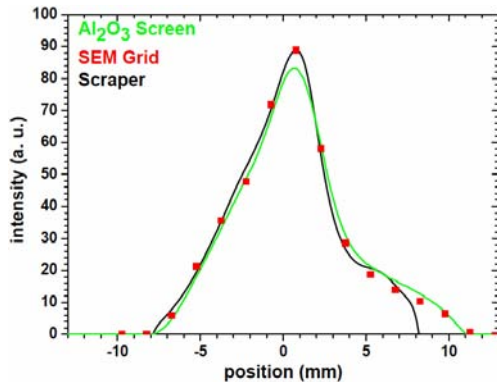


Figure 7: Comparison of the beam profile width for the three different beam diagnostic methods: first macro pulse irradiated on  $\text{Al}_2\text{O}_3$  screen (blue), SEM-grid (red) and scraper scan (black) (beam parameters as Fig. 6).

**Instrumentation**

The beam profiles obtained with the three different methods are in good agreement (Fig. 7). For the scraper scan, the difference in the profile is the result of the used smoothing algorithm (Gaussian FFT) and beam fluctuations during the measurements. To reduce this error measurements with more stable ion beam conditions have to be performed.

The calculated  $\sigma$  (in the  $\pm 7$  mm region) is comparable for the  $\text{Al}_2\text{O}_3$  screen ( $\sigma=2.82\text{mm}$ ) and the scraper scan ( $\sigma=2.81\text{mm}$ ). The difference for the SEM-grid ( $\sigma=3.0\text{mm}$ ) might be correlated to the poor spatial resolution of this method (1.5mm).

*Spectroscopic studies*

The luminescence spectra of the six different scintillation screens ( $\text{Al}_2\text{O}_3$ ,  $\text{ZrO}_2:\text{Mg}$ , Herasil,  $\text{Al}_2\text{O}_3:\text{Cr}$ ,  $\text{ZrO}_2:\text{Y}$ , AlN) were studied using a high intensity  $\text{U}^{28+}$  ion beam (up to 100 macro pulses). In the following section we will concentrate on the spectroscopic changes during irradiation of Herasil, AlN and  $\text{Al}_2\text{O}_3:\text{Cr}$  scintillating screens.

The most prominent changes in the emitted light occur in the quartz glass (Herasil). The obtained spectra (Fig. 8 and Fig. 9) change significantly with the increasing number of macro pulses irradiated on the sample.

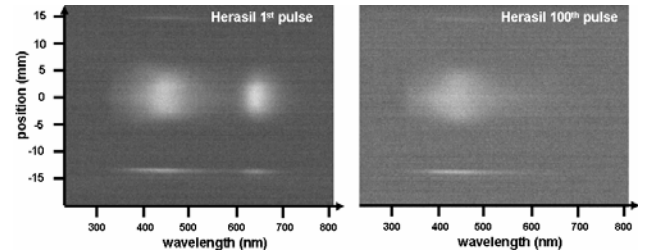


Figure 8: Spectroscopic beam image obtained for Herasil sample at 1<sup>st</sup> and 100<sup>th</sup> pulse of the high current  $\text{U}^{28+}$  ion beam. Beam parameters:  $5.2 \cdot 10^{10}$  ppp at 4.8 MeV/u, 0.8 ms pulse length and 0.5 Hz repetition rate. Due to the low intensity of the right image, the brightness was adjusted.

The intensity of the broad band around 440 nm decreases with irradiation time, while the band at around 640 nm completely vanishes after ten pulses.

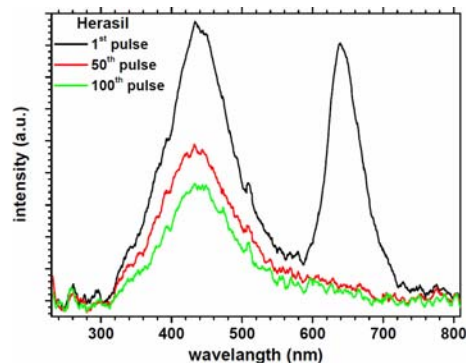


Figure 9: Luminescence spectra of Herasil obtained for the 1<sup>st</sup> (black), 50<sup>th</sup> (red) and 100<sup>th</sup> (green) macro pulse (beam parameters as Fig. 8).

Also for the AlN sample significant changes occurred in the emitted light spectra. The luminescence spectra (Fig. 10) show a broad band emission with the centre at 370 nm which can be related to imperfections in the sample created during its growth as discussed in [6]. The intensity of the peak rapidly decreases with the successive pulses.

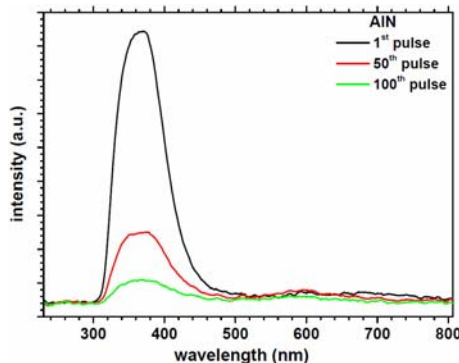


Figure 10: Luminescence spectra of AlN recorded during the 1<sup>st</sup> (black), 50<sup>th</sup> (red) and 100<sup>th</sup> (green) macro pulse (beam parameters as Fig. 8).

After several macro pulses the spectroscopic picture shows that no more transitions are detected from the middle part of the sample (Fig. 11). This suggests strong and permanent damages of the sample due to irradiation (e.g. heating of the sample) as shown in Fig 1.

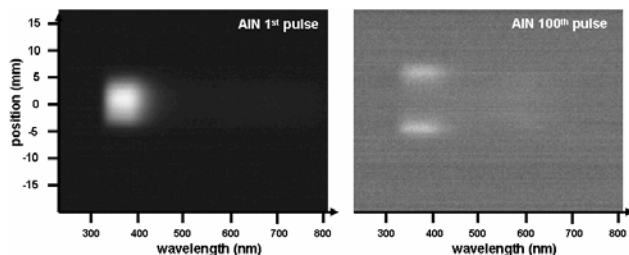


Figure 11: Spectroscopic pictures of AlN sample at 1<sup>st</sup> (left) and the 100<sup>th</sup> (right) pulse. Due to the low intensity of the right image, the brightness was adjusted (beam parameters as Fig. 8).

The projected beam profiles for AlN, obtained along imaging axes, change dramatically with the integrated particle number and can lead to wrong profile measurements (see Fig. 12).

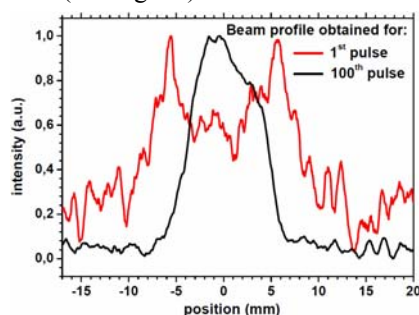


Figure 12: Beam profile obtained along imaging axis for AlN recorded during the 1<sup>st</sup> (black) and 100<sup>th</sup> (red) macro pulse (beam parameters as Fig. 8).

## Instrumentation

Cr doped Al<sub>2</sub>O<sub>3</sub> is often used for the adjustment of the ion beam at accelerating facilities.

The luminescence spectra show (Fig. 13) a clear and sharp line at 693 nm. This transition can be attributed to the relaxation from the excited <sup>2</sup>E-state of the Cr<sup>3+</sup> ions which produce R-line emission in this spectral region [7]. The intensity of the observed peak strongly decreases with the successive pulses and surface modification occurs (see Fig. 1).

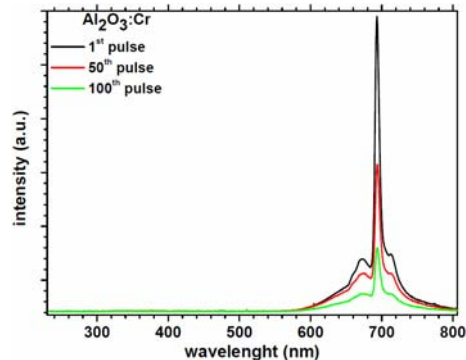


Figure 13: Luminescence spectra of Al<sub>2</sub>O<sub>3</sub>:Cr recorded during the 1<sup>st</sup> (black), 50<sup>th</sup> (red) and 100<sup>th</sup> (green) macro pulse (beam parameters as Fig. 8).

## CONCLUSION

Several scintillating materials were investigated under irradiation with high current ion beams. The obtained beam width differs by a factor of two for different materials. The investigated properties are influenced by the temperature of the applied material. This knowledge is essential for choosing a well suited material for the precise emittance measurements with the pepper-pot method.

In the case of Al<sub>2</sub>O<sub>3</sub> comparison of the obtained beam profile width for three different diagnostic methods show a good agreement. The advantage of the optical method is that it provides a big amount of detailed information on the beam particle distribution with much higher spatial resolution.

Spectroscopic studies performed on inorganic scintillators show that damages, generated during ion irradiation, lead to significant changes in the emitted light spectra. Additionally, the beam profile may vary strongly with the number of macro pulses as shown in Fig. 6 and Fig. 12. Both effects limit the performance of the detectors over operation time and more detailed investigations on these topics have to be performed. For high current ion beams the radiation resistance of the sample is critical.

## ACKNOWLEDGMENT

The authors would like to thank Walter Tutsch from PCO AG, Germany for the possibility to use a high performance CCD camera and Klaus Höhne for useful discussion.

## REFERENCES

- [1] T. Hoffmann et al., “Emittance measurements at the new UNILAC pre-stripper using a pepper-pot with a PC-controlled CCD camera”; <http://www-bd.gsi.de>.
- [2] E. Gütlich et al., “Scintillation screen investigations for high current ion beams”, IEEE Transactions on Nuclear Science (accepted for publication in June 2010).
- [3] P. Forck, “Lecture notes on Beam Instrumentation and Diagnostics”, Joint Universities Accelerator School (JUAS 2010); <http://www-bd.gsi.de>.
- [4] E. Gütlich et al., “High current ion beam investigation on inorganic scintillation screens”, DIPAC’09; <http://www.pcapacworkshop.org>.
- [5] R. Haseitl et al., “BeamView – A Data Acquisition System for Optical Beam Instrumentation”, PC@PAC’08; <http://www.JACoW.org>.
- [6] S. W. Choi et al., “Emission spectra from AlN and GaN doped with rare earth elements”, Journal of Alloys and Compounds 408-412 (2006).
- [7] S. W. S. McKeever et al., “Characterisation of Al<sub>2</sub>O<sub>3</sub> for use in thermally and optically stimulated luminescence dosimetry”, Radiation Protection Dosimetry 84 (1999).